PHYSICAL REVIEW A VOLUME 43, NUMBER 9 1 MAY 1991

Cascade decays of hollow ions

Gaber Omar
Department of Physics, Ain Shams University, Abbassia, Cairo, Egypt

Yukap Hahn
Department of Physics, University of Connecticut, Storrs, Connecticut 06269
(Received 13 August 1990)

A multiple-electron-emission process for atoms with one or more inner-shell vacancies is treated using the radiative- and Auger-electron-emission cascade model, in which inner-shell holes are assumed to decay by sequentially emitting radiations and/or Auger electrons. Such hollow ions are produced by synchrotron irradiation of atomic targets and in ion-surface interactions with multiple-electron transfers. The final charge-state distribution is determined by the Auger and radiative branching ratios at each stage of the decay sequence. At intermediate stages of cascade, hollow ions with more than one hole in different ionization stages are created. The Ne, Mg, and Fe^{14+} ions with the initial $1s$, $2s$, and $2p$ vacancies are considered in detail, and the core charge dependence of the maximum charge state is studied. The hollow Mg ion with double initial $1s$ holes is analyzed, and the result compared with that for the case of one $1s$ hole. The peak is shifted more than two units to a higher degree of ionization. The correlated shake-off and shake-up multiple-electron processes are not considered, but they are expected to cause further shifts.

I. INTRODUCTION

Availability of intense synchrotron light sources provides a powerful tool to study atomic structure and collision processes.[1-3] Together with the multiply charged ion sources, both neutral and charged targets along a given isoelectronic sequence can be used to investigate the correlation and scaling of various transition probabilities. In particular, hollow ions with one or more inner-shell vacancies may be created by a variety of reactions, and decay of such ions provides detailed information on the structure of many exotic ionic states that are otherwise difficult to create. There are several ways by which inner-shell holes may be created: (a) electron-ion collisions, (b) ion-atom collisions, (c) synchrotron radiation-ion interaction, and (d) ion-surface interaction.

The decay products of atoms with initial inner-shell holes were studied during the 1960s by Krause, Carlson, and others,[4] both experimentally and theoretically. A simple model based on the sudden approximation was used to interpret the data, in which outer-shell electrons are assumed to be affected by a sudden change in the core charge distribution as the inner-shell holes are filled by upper-level electrons during the cascade. This shake-off process involved many decay routes, which were treated by a random Monte Carlo procedure. The model was able to reproduce the data reasonably well, and it was concluded that the correlated multi-electron (CME) shake-off and shake-up processes, involving simultaneously three or more electrons, contribute significantly to the higher charge states. More recently, Mirakhmedor and Parilis[5] also carried out a detailed analysis using a similar procedure.

In this paper, we analyze the decay of hollow ions assuming that the only decay mechanisms involved are the simple, lowest-order radiative and Auger emissions in cascade (RAC). The CME effects which may lead to simultaneous multiple ionization and excitations will be neglected, mainly because a consistent theoretical formulation is lacking at present. Their effect is presumably at the 10% to 20% level overall, but more importantly, tends to skew the final charge-state distribution toward higher charges.

Of special interest here are the decay processes of hollow ions created by synchrotron light irradiation of atomic and ionic targets. The experiments on Ar and Xe atoms have been carried out, and their charge-state distributions have been reported.[6,7] The analysis of these systems is extremely complicated, however. Once a hole is created in the target system, it will usually decay by cascade, emitting electromagnetic radiations and Auger electrons, as dictated by their emission branching ratios at each intermediate state, until the energetically stable final states are reached (or metastable because of relevant selection rules). Therefore the final charge-state distribution depends critically on the electron-electron correlations at each stage of the cascade, so as to control the subsequent decay modes. Preliminary to the analysis of the argon system, with extremely complicated decay schemes for the initial $1s$, $2s$, and $2p$ hole states, we examine here the much simpler systems of Mg and Fe^{14+}, as well as Ne, to learn first the intricacies of the photo-Auger-ionization (PAI) processes. Even then, the calculations are very long and tedious; there are many radiative and Auger branching ratios to calculate, as explained in detail in Secs. III and IV. The dependence of the charge-state distribution on the core charge Z_c is also elucidated.

Cascade decay of more exotic ions with multiple initial holes is also treated by the method developed here, the

case of $Mg^{2+}(\overline{1s^2})$ containing two $1s$ holes. Recently, an experiment was reported[8] in which an Ar^{17+} beam was incident on a metallic surface. Multiple electron transfer to Rydberg states of the projectile ion took place, forming hollow ions with more than one inner-shell vacancy. Such experimental techniques, under controlled conditions, can open up a new area of inner-shell research, in which more than one initial hole is generated.

II. THEORY

To treat the decay of an atom or ion with one or more initial inner-shell holes, we construct a simple RAC model.[7,8] Thus the process is described schematically as

$$\gamma + A^{Z_l} \rightarrow A^{Z_I}(\bar{i})$$

or

$$\gamma + A^{Z_L} \rightarrow A^{Z_I+l}(\bar{i}), \quad \bar{i}=\overline{n_h l_h}$$

where, for example,

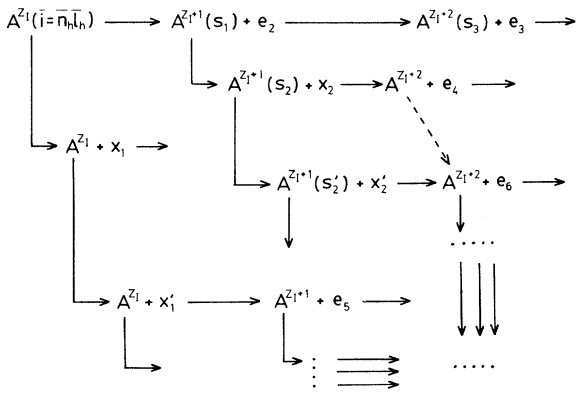

The vertical downward transitions are radiative emissions and the horizontal transitions involve Auger emissions. The final charge-state distribution is given by

$$P(Z_c,Z_I,\bar{i};Z_f) \equiv P(Z_f) = \sum_\alpha P_\alpha(Z_f;\alpha=p_i,q_i) , \tag{1}$$

where label α denotes the particular cascade path followed in reaching the final charge states Z_f, and

$$P_\alpha = \prod_{i=1}^{Z_f-Z_I} (\omega^{p_i}\xi^{q_i}) . \tag{2}$$

In the product for F_α, we have the constraint

$$\sum_i q_i = Z_f - Z_I \tag{3}$$

and p_i and q_i assume the values

$$p_i = 0,1,2,\ldots , \tag{4}$$

$$q_i = 1,2,3,\ldots \ (q_i=0 \text{ omitted for the final x rays}) . \tag{5}$$

Furthermore, the notation used here for the radiative and Auger cascade branching ratios is

$$\omega^{p_i} \equiv \omega(s_{p_i} \rightarrow s_{p_i-1})\omega(s_{p_i-1} \rightarrow s_{p_i-2}) \cdots \omega(s_1 \rightarrow f) , \tag{6}$$

$$\xi^{q_i} \equiv \xi(s_{q_i} \rightarrow s_{q_i-1})\xi(s_{q_i-1} \rightarrow s_{q_i-2}) \cdots \xi(s_1 \rightarrow g) , \tag{7}$$

where

$$\omega(s \rightarrow f) = \frac{A_r(s \rightarrow f)}{\Gamma(s)} \tag{8}$$

and

$$\xi(s \rightarrow g) = \frac{A_a(s \rightarrow g)}{\Gamma(s)} \tag{9}$$

are the partial fluorescence yields and partial Auger yields, respectively. As usual, the total width of the state s is given in terms of the radiative and Auger transition probabilities A_r and A_a

$$\Gamma(s) = \Gamma_a(s) + \Gamma_r(s) , \tag{10}$$

$$\Gamma_a(s) = \sum_{s'} A_a(s \rightarrow s') , \tag{11}$$

$$\Gamma_r(s) = \sum_{s''} A_r(s \rightarrow s'') . \tag{12}$$

To understand the result of the explicit calculation presented in the next section, it is useful to recall[9-11] the scaling properties of A_a and A_r; for intrashell transitions ($\Delta n_t = 0$),

$$A_a \sim Z^{1/2} \tag{13}$$

and

$$A_r \sim Z^1 , \tag{14}$$

while for intershell processes ($\Delta n_t \neq 0$)

$$A_a \sim Z^0 \tag{15}$$

and

$$A_r \sim Z^4 , \tag{16}$$

where Z is some effective charge seen by the active electrons involved in the transitions. The above scaling laws are valid only when Z is large ($Z \geq 5$). Therefore, for nearly neutral ions with one or two holes, special care is needed in applying them; the relationships are more applicable for the later stages of the Auger cascades.

For atoms with a hole in the n_h shell and the uppermost occupied shell n_M, where $n_M - n_h \geq 2$, the decay paths are generally very involved, and it is nontrivial to keep track of all the decay paths which end up with the Z_f-ionized ion. The RAC model, as described by Eqs. (1)–(7) above, may be too cumbersome for systems with a large number of electrons, and explicit calculations of some simple systems such as Ne, Mg, and Ar are eventually needed in developing a simpler approach. We neglect in the RAC model those decay transitions involving correlated electron pairs. Inclusion of such processes unduly complicates the calculation, but their contribution is not expected to be important; the correlated transitions can be incorporated by the configuration mixing procedure, but the overall effect of the mixing usually

cancels out in the total rates, although the individual rates are sometimes strongly affected.

III. APPLICATIONS

The calculation is carried out in the angular-momentum average (AMA) approximation, using configuration-averaged energies. The angular-momentum-coupled calculation will increase the work manyfold without seriously adding anything new. The relative charge distribution of interest here is not expected to be sensitive to angular-momentum coupling. Since both ω and ξ involve ratios of the A_r and A_a, the P's evaluated with AMA (for A_a, A_r) should provide reasonable and realistic distribution.

We have used our MATRIX code in the evaluation of A_a and A_r, with single configuration Hartree-Fock (HF) wave functions for the orbitals involved. No energy adjustments were made in A_r, which could introduce additional errors in some cases, especially when transition energies are small and so are the corresponding A_r. This is also not expected to affect much the final results.

A. Ne with one 1s or one 2s hole

We start with the simplest picture of the RAC. The photoexcitation of the Ne atom creates an inner-shell ($1s$) hole as one electron is raised either to an empty bound excited state or to continuum.

1. Excitation of the inner-shell electrons to upper bound states

In this case, the transitions involved are $1s\rightarrow 3p$, $1s\rightarrow 4p, \ldots$ and $2s\rightarrow 3p$, with the resulting configurations $1s2s^22p^63p$, $1s2s^22p^64p, \ldots$ and $1s^22s2p^63p$, etc.

The study of cascade for the first configuration $d=1s2s^22p^63p$, for example, is treated by the following scheme:

Auger transition	Rate	
$1s^22p^63p+e_1$	$A_a(l_c=0)=0.4420(+14)$	(S1)
$1s^22s2p^53p+e_1$	$A_a(l_c=1)=0.1169(+15)$	(S2)
$1s^22s2p^6+e_1$	$A_a(l_c=1)=0.1909(+12)$	(S3)
$1s^22s^22p^43p+e_1$	$A_a(l_c=0)=0.1760(+14)$	(S4)
	$A_a(l_c=2)=0.2212(+15)$	
$1s^22s^22p^5+e_1$	$A_a(l_c=0)=0.5751(+11)$	(S5)
	$A_a(l_c=2)=0.6980(+12)$	
Radiative transition	**Rate**	
$1s^22s^22p^6+\gamma$	$A_r=0.1080(+11)$	(S6)
$1s^22s^22p^53p+\gamma$	$A_r=0.7293(+13)$	(S7)
$1s2s^22p^63s+\gamma$	$A_r=0.4535(+8)$	(S8)

where A_a, A_r are the Auger and radiative rates in the AMA scheme and are given in units of $\sec^{-1}$. Of course, the first-generation electrons (e_1) have different energies for states (S1)–(S5) and similarly the photons γ_1 have different energies for states (S6), (S7), and (S8). For this particular state (d), we have to consider now the second-generation decays of all eight new states created, some with more than one hole. States (S3), (S4), and (S5) are stable and lead to Ne^{1+}, with probability $P(Ne^{1+})=\sum_{d'=3,4,5}\xi(d\rightarrow d')=0.587$, and states (S6) and (S7) are stable but lead to Ne^{0+} with probability $P(Ne^{0+})=\omega(d\rightarrow S6,S7)=0.018$. We neglect state (S8) because its A_r is very small. The next step is the decay of state (S1) which is still unstable to Auger decay. This state decays as

Auger transition	Rate	
$1s^22s2p^5+e_2$	$A_a(l_c=0)=0.2815(+14)$	(S9)
	$A_a(l_c=2)=6.1349(+15)$	
Radiative transition	**Rate**	
$1s^22s2p^6+h\nu$	$A_r=0.1114(+16)$	(S10)
$1s^22s2p^53p+h\nu$	$A_r=0.9371(+11)$	(S11)

State (S9) is stable and leads to Ne^{2+}, with the probability $P(Ne)^{2+}=\xi(d\rightarrow S1)\xi(S1\rightarrow S9)=(0.108)(1.0)=0.108$, and states (S10) and (S11) lead to Ne^{1+} but their radiative branching ratios are very small. In addition, state (S2), $1s^22s2p^53p$, is still unstable and decays as

Auger transition	Rate	
$1s^22s^22p^4+e_2$	$A_a(l_c=0)=0.1422(+14)$	(S12)
	$A_a(l_c=2)=0.2525(+14)$	
Radiative transition	**Rate**	
$1s^22s^22p^5+h\nu'$	$A_r=0.5722(+9)$	(S13)
$1s^22s^22p^43p+h\nu'$	$A_r=0.1172(+11)$	(S14)

State (S12) represents Ne^{2+} which is formed with probability $P(Ne^{2+})$, where $P(Ne^{2+})=\xi(d\rightarrow S2)\xi(S2\rightarrow S12)=(0.286)(1.0)=0.286$, and states (S3) and (S4) decay to Ne^{1+} with small Auger branching ratios.

Obviously, states (S9) and (S10), . . . may further decay and we have the third-generation cascades to consider, and so forth, until all the states created are stable.

The final result of the decay of the photo excited $Ne(1s2s^22p^63p)$ gives rise to Ne^{0+},Ne^{1+},Ne^{2+} with the probabilities $P(Ne^{0+})=0.018$, $P(Ne^{1+})=0.587$, and $P(Ne^{2+})=0.394$. These probabilities are drawn as vertical lines in Fig. 1(a).

2. Transition to continuum state (initial ionization)

In this case the initial state thus formed has the configuration $1s2s^22p^6$. The decay scheme in this case is simpler, because there is a lesser number of electrons in the orbits above the hole. This hollow ion will decay as follows:

Anger transition	Rate	
$1s^22p^6+e_2$	$A_a(l_c=0)=0.5585(+14)$	(S1′)
$1s^22s2p^5+e_2$	$A_a(l_c=1)=0.9075(+14)$	(S2′)
$1s^22s^22p^4+e_2$	$A_a(l_c=0)=0.1207(+14)$	(S3′)
	$A_a(l_c=2)=0.1629(+15)$	
Radiative transition	**Rate**	
$1s^22s^22p^5+h\nu$	$A_r=0.6696(+13)$	(S4′)

States (S1'), (S2'), (S3') are stable and lead to Ne^{2+}, with probability $P(Ne^{2+})=\xi(d'\rightarrow S1',S2',S3')=0.98$ and state (S4') leads to Ne^{1+} with probability $P(Ne^{1+})=\omega(d'\rightarrow S4')=0.02$. The charge-state distribution of Ne to Ne^{1+} and Ne^{2+} is represented in Fig. 1(b). Experimental data shown in Figs. 1(b) and 1(c) are from Ref. 4. As noted earlier, the RAC predicts the final charge-state distribution which tends to miss the higher charge states because of the neglect of the shake-off contribution. However, the straightforward RAC contribution is now isolated, and improved theory with the shake-off should account for the discrepancy.

The Auger and radiative decay probabilities generated in this work are evaluated in the angular-momentum-averaged scheme, in order to simplify the work to a manageable level. This is necessitated by the magnitude of the calculation involved. However, we expect from our previous experience that this will not cause serious distortion in the final charge distribution we obtain.

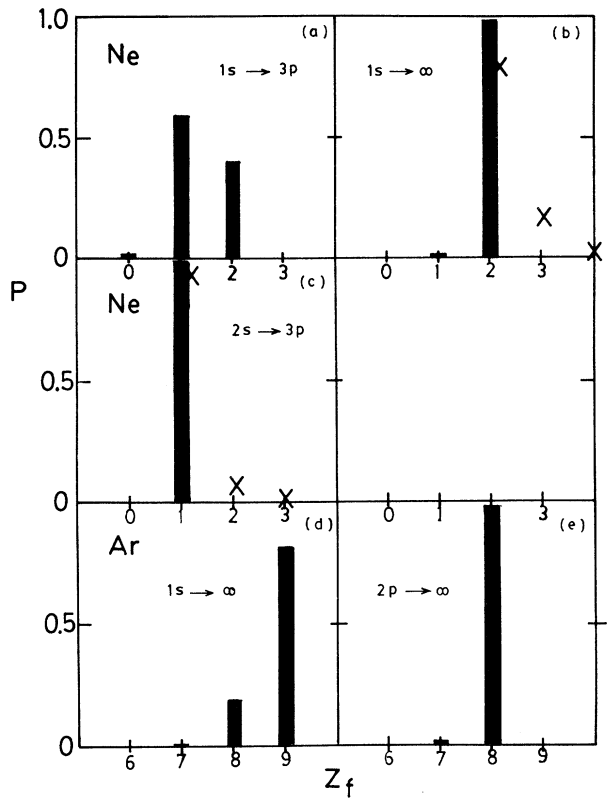

FIG. 1. Charge-state distribution for the photoexcited Ne atom and Ar^{6+} ion. The probabilities (P) for ions with final ionization (Z_f) are represented by vertical lines. Different modes of initial photoexcitation are given; for example, $1s\rightarrow 3p$ denotes the case of initial photoexcitation of the $1s$ electron to the $3p$ orbital. The experimental data are from Ref. 4. The higher charge states are not predicted by the RAC, and the discrepancy is presumably due to the neglect of the shake-off contribution.

B. Mg ions with one hole in 1s, 2s, and 2p

Although the system contains only two electrons more than neon, one $1s$ hole leads to a much more complicated decay scheme. The decay of $d=1s2s^22p^63s^23p$ of the photoexcited Mg atom, for example, is described as

Auger transition	Rate	
$1s^22p^63s^23p+e_1$	$A_a(l_c=0)=0.5388(+14)$	(S1)
$1s^22s2p^53s^23p+e_1$	$A_a(l_c=1)=01504(+15)$	(S2)
$1s^22s2p^63s3p+e_1$	$A_a(l_c=0)=0.5338(+13)$	(S3)
$1s^22s2p^63s^2+e_1$	$A_a(l_c=1)=0.8144(+12)$	(S4)
$1s^22s^22p^43s^23p+e_1$	$A_a(l_c=0)=0.2415(+14)$	(S5)
$1s^22s^22p^53s3p+e_1$	$A_a(l_c=2)=0.3032(+15)$	
	$A_a(lc=1)=0.6718(+13)$	(S6)
$1s^22s^22p^53s^2+e_1$	$A_a(l_c=0)=0.5142(+12)$	(S7)
	$A_a(l_c=2)=0.6146(+13)$	
$1s^22s^22p^63p+e_1$	$A_a(l_c=0)=0.1316(+12)$	(S8)
$1s^22s^22p^63s+e_1$	$A_a(l_c=1)=0.3597(+11)$	(S9)

Radiative transition	Rate	
$1s^22s^22p^53s^23p+\gamma$	$A_r=0.1789(+14)$	(S10)
$1s^22s^22p^63s^2+\gamma$	$A_r=0.8780(+11)$	(S11)

State (S11) of Mg^{0+} is formed directly from state (d), with probability $P(Mg^{0+})=\omega(d\rightarrow S11)=1.54\times10^{-4}$, while states (S8) and (S9) give stable Mg^{1+} with probability $P(Mg^{1+})=\xi(d\rightarrow S8,S9)=2.944\times10^{-4}$. State (S10) further decays and gives both Mg^{0+} and Mg^{1+}. This is indicated in Table I, which also contains states (S3),(S4),(S5),(S6),(S7) leading to Mg^{1+} and Mg^{2+}, while states (S1) and (S2) are allowed to decay in three successive steps to give the final Mg^{2+} and Mg^{3+}. As a more detailed explanation of the cascades, we show schematically the decay of state (d) via state (S2),

$$1s2s^22p^63s^23p \quad \text{(d)}$$
$$\downarrow$$
$$1s^22s2s^53s^23p \quad \text{(S2)}$$
$$\downarrow$$
$$1s^22s^22p^43s3p \quad \text{(S2')}$$
$$\downarrow$$
$$1s^22s^22p^5 \quad \text{(S2')}.$$

The probability of forming Mg^{3+} from (d) via state (S2) is given by

$$P(Mg^{3+})=\xi(d\rightarrow S2)\xi(S2\rightarrow S2')\xi(S2'\rightarrow S2') .$$

Similar discussion can be given on the decay of $1s2s^22p^63s^2$, in which the $1s$ electron is liberated initially during the photoexcitation of the Mg atom. The ionic charge distribution starts from Mg^{1+} in this case, as shown in Fig. 2(b).

The charge-state distribution due to the decay of Mg with the $2s$ initial hole is also calculated using the same RAC model. The results are represented graphically in Figs. 2(c) and 2(d). The $2p$ electron excitation is studied in three cases: (i) transition of the $2p$ electron to $4s$, (ii) transition of the $2p$ electron to $3d$, and (iii) transition of

TABLE I. The probabilities of formation of Mg in different charge states due to the decay of states (S1)–(S11), which come from $1s2s^22p^63s^23p$.

State	Mg^{0+}	Mg^{1+}	Mg^{2+}	Mg^{3+}
(S11)	0.0002			
(S10)	0.0003	0.0314		
(S8,S9)		0.0003		
(S7)		0.0115	0.0002	
(S6)		small	0.0118	
(S5)		small	0.575	
(S4)		small	0.0014	
(S3)		small	0.0094	
(S2)			0.0059	0.258
(S1)			small	0.0946
Total	0.0005	0.0432	0.6037	0.3526

the $2p$ electron to continuum. The probabilities of Mg^{Z_f+} charge states for these three cases are respectively given in Figs. 2(e) and 2(f).

C. Hollow Fe^{14+}

According to the scaling properties of A_a and A_r, given by Eqs. (13)–(16), the A_r's play a more important role as Z_c is increased. Therefore we expect that the charge-state distribution of Mg-like Fe ions will be shifted toward lower Z than that of the Mg atom. However, the extent of the shift and its trends cannot be predicted *a priori*, until the detailed calculation is carried out. All the cases we studied for Mg are also considered for Fe^{14+}. The results are summarized in Figs. 3(a) and 3(b) for the initial $1s$ hole, Figs. 3(c) and 3(d) for the $2s$ hole, and Figs. 3(e) and 3(f) for the $2p$ hole. To further facilitate the comparison between Mg and Fe^{14+}, we present all the probabilities of charge-state distribution of Fe^{14+},Fe^{15+},Fe^{16+} generated by the decay of states (S1) to (S11) which come from the initial hole state $1s2s^22p^63s^23p$ of photoexcited Fe^{14+}.

From Tables I and II we see that states (S1) and (S2) are allowed to decay to the third generation Mg^{3+} but energetically forbidden to produce Fe^{17+}. We also note

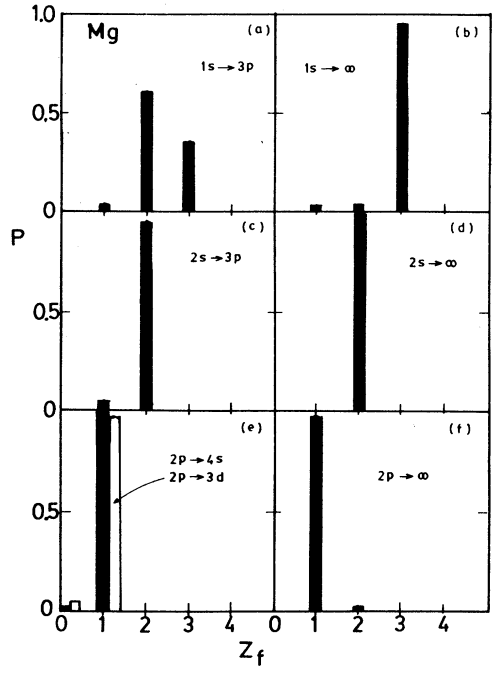

FIG. 2. Same as Fig. 1 but for the photoexcited Mg atom. Both cases with the removed electron occupying the upper excited states and to the continuum are treated.

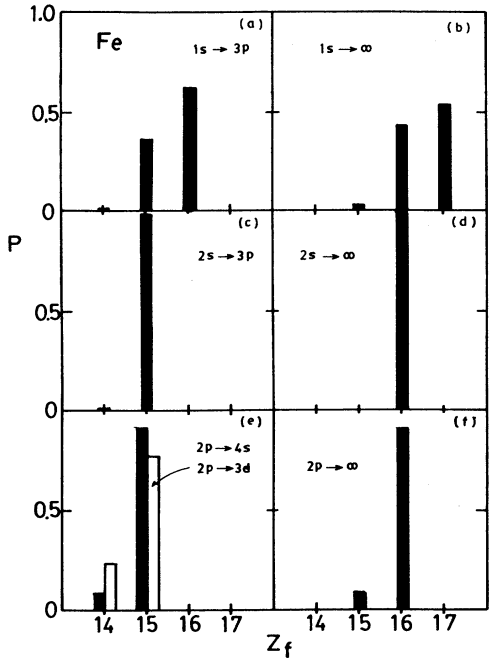

FIG. 3. Same as Fig. 1 but for the photoexcited Fe^{14+} ions with the initial holes in $1s$, $2s$, and $2p$. Note the shift in the peak distribution toward the initial charge, as compared to the Mg case of Fig. 2.

TABLE II. Same as Table I but for Fe^{14+}.

State	Fe^{14+}	Fe^{15+}	Fe^{16+}	Fe^{17+}
(S11)	0.0103			
(S10)	0.005	0.347		
(S8,S9)		0.002		
(S7)		0.002	0.018	
(S6)		0.0004	0.0216	
(S5)		0.011	0.368	
(S4)			0.005	
(S3)		0.0006	0.0154	
(S2)			0.149	
(S1)			0.046	
Total	0.0153	0.363	0.623	0.000

that there seems to be an anomalous behavior in the Mg($\overline{1s}$) case as compared with Fe($\overline{1s}$), Figs. 1(b) and 2(b). The charge state Mg^{2+} is hardly produced, while Fe^{16+} production is much higher.

D. Hollow Ar^{6+}

To further clarify the strange behavior noted above in the $Mg^{+}(\overline{1s})$ case, we studied the $Ar^{6+}(\overline{1s})$ system which is expected to have the behavior intermediate between Mg and Fe. The results shows that indeed Ar^{6+} is similar to $Fe^{14+}(\overline{1s})$, with less shift in the peak distribution to higher charge states than in Fe^{14+}. Therefore the anomaly in Mg^{+} is presumably caused by the unusually small Auger rate (due to cancellation of the matrix element) in the decay of the final state $1s^2 2s^2 2p^5 3s^2$, which was reached from $1s2s^2 2p^6 3s^2$ by radiative transition. The charge-state distribution for the photoexcited Ar^{6+} with one $1s$ hole, leading to Ar^{7+} and subsequent decays, is shown in Fig. 1(d).

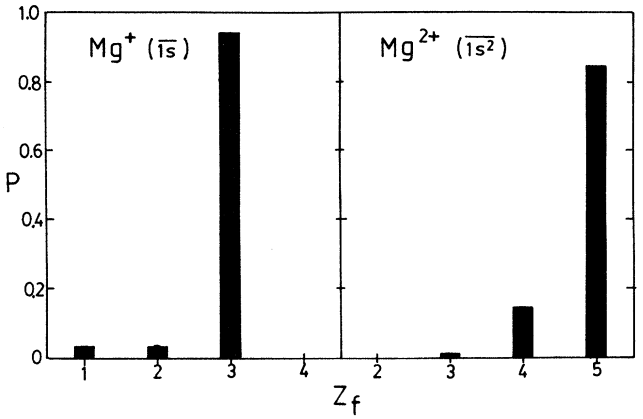

FIG. 4. Same as Fig. 1 but for the hollow Mg atom with two ($1s$) holes. The result for the single initial $1s$ hole is also shown for comparison. Apparently, the two-hole case produces more than double the number of electrons emitted.

IV. HOLLOW Mg IONS WITH TWO $1s$ HOLES

The recent experiment on ion-surface interaction showed that ions with multiple inner-shell holes can be created by multiple charge exchanges which preferentially fill the upper shells. Detailed spectroscopic information can be obtained for exotic atoms and ions for such systems with multiple inner-shell holes. In particular, the final charge-state distribution for the individual hollow configuration would be of much interest. In view of the fact that the systems studied in the preceding sections also involve multiple inner-shell holes in the intermediate stages of cascade decay, the basic physics involved in hollow atoms is similar and closely related to that of Sec. III.

As a first attempt to analyze the charge distribution of hollow atoms with many holes, we consider here $Mg^{2+}(\overline{1s^2})$ with two $1s$ holes initially. The results here then can be directly compared with that of Sec. III B, where $Mg^{+}(\overline{1s})$ with one hole was analyzed. The decay scheme in this case is

Auger transition	Rate	
$1s2p^6 3s^2 + e_1$	$A_a(l_c=0)=0.1116(+15)$	(S1)
$1s2p2p^5 3s^2 + e_1$	$A_a(l_c=1)=0.2505(+15)$	(S2)
$1s2s2p^6 3s + e_1$	$A_a(l_c=0)=0.1206(+14)$	(S3)
$1s2s^2 2p^4 3s^2 + e_1$	$A_a(l_c=0)=0.5952(+14)$ $A_a(l_c=2)=0.7710(+15)$	(S4)
$1s2s^2 2p^5 3s + e_1$	$A_a(l_c=1)=0.2442(+14)$	(S5)
$1s2s^2 2p^6 + e_1$	$A_a(l_c=0)=0.6368(+12)$	(S6)

Radiative transition	Rate	
$1s2s^2 2p^5 3s^2 + \gamma'$	$A_r=0.5978(+14)$	(S7)

We now compare the distribution obtained for the two hole ions with that for $Mg^{+}(\overline{1s})$, as shown in Fig. 4. Although we started out with two $1s$ holes, the final peak value is more than doubled and shifted to a higher charge state for the $Mg^{2+}(\overline{1s^2})$ case. It is therefore reasonable to expect that, in general, the degree of ionization for the final states will be much higher than that one expects from a simple scaling for atoms with multiple holes. Much work is yet needed to understand more fully the decaying behavior of hollow atoms.

Furthermore, in actual experiment, whether holes are created by synchrotron radiation, by electron impact, or by ion-atom collisions, the final charge-state distribution may be due to a combination of the different number of holes created. The overall distribution in such cases require superposition of the results obtained in Secs. III and IV. Such analysis provides information on the physical mechanisms for the creation of different hollow states.

The RAC model may be easily applied to other exotic hollow ions, such as the Ar ions with nearly empty K and L shells, but with several electrons in the M and N shells. The decay of such ions is under investigation to predict the final state charge distribution.

V. SUMMARY AND DISCUSSION

The peaks for the charge-state distribution for ions of given isoelectric sequence shift toward smaller Z_f as Z_c increases. This is principally due to the increased role played by A_r as compared to A_a. (For small Z, $A_r \ll A_a$, but A_r increases rapidly with Z.) No experiments are available for the ions considered here, i.e., Mg, Fe^{14+}, and Ar^{6+}. However, they are some of the simplest systems in which the cascade decay routes are nontrivial, and provide a testing ground for the RAC model. On the other hand, the experimental data on argon atoms have been available for several years, and this system will be analyzed[12] using the same RAC model.

As noted earlier, the present study is incomplete because of the omission of the shake-off and shake-up contributions. These processes are difficult to incorporate, since they require correlated multiple-electron (three-electron, etc.) vertices to represent the simultaneous multistate transitions. A simple theoretical procedure of taking an overlap of the wave functions, before and after the

inner-shell vacancy decay, as was done in the sudden approximation, may not be consistent within the RAC model. The problem of double-counting of the cascades should also be addressed in a more careful treatment. Currently, the correct shake-off theory does not exist. Nevertheless, the present calculation isolates the RAC contribution, thus clearly indicating the need for the CME effect. The RAC model used here has to be modified in such a way that the CME effect comes in at every step of the cascade, where the availability of energies for such decay has to be tested. This problem is under investigation.

In addition to the final charge-state distribution calculated in this paper, the Auger-electron and x-ray spectra in the decay of inner-shell vacancies are also of interest, as they provide additional information on the various intermediate states which are formed during the cascade. This calculation is in progress and will be reported elsewhere.[12]

From the experience gained in the present work, it is clear that applications of RAC directly to systems more complicated than Ar will be prohibitive. The explicit calculation[13] for argon, together with the result of this paper, will be useful in developing a simpler model to treat ions with a large number of electrons,[7] such as Kr and Xe. Furthermore, ions with multiple initial vacancies but with a lesser number of electrons in the outer shells may be investigated using the same RAC model.[8]

ACKNOWLEDGMENTS

The work reported here was partially supported by a U.S. Department of Energy grant and also by a University of Connecticut Research Foundation grant. One of the authors (G.O.) wishes to thank the Physics Department of the University of Connecticut for hospitality and for the use of the University Computer Center.

[1]K. W. Jones *et al.*, Comments At. Mol. Phys. **20**, 1 (1987).
[2]P. Zimmermann, Comments At. Mol. Phys. **23**, 45 (1989).
[3]F. C. Farnoux, J. Phys. (Paris) Suppl. **C7**, 3 (1988).
[4]T. A. Carlson and M. O. Krause, Phys. Rev. **140**, A1057 (1965); **158**, 18 (1967).
[5]M. N. Mirakhmedor and E. S. Parilis, J. Phys. B **21**, 775 (1988).
[6]D. A. Church *et al.*, Phys. Rev. A **36**, 2487 (1987).
[7]J. C. Levin, in *Proceedings of the 16th International Conference on the Physics of Electronic and Atomic Collisions, New York, 1989,* AIP Conf. Proc. No. 205, edited by A. Dalgarno, R. S. Freund, M. S. Lubell, and T. B. Lucatorto (AIP, New York, 1990), p. 176.
[8]J. P. Briand *et al.*, Phys. Rev. Lett. **65**, 159 (1990).
[9]Y. Hahn, Phys. Lett. **67A**, 345 (1978).
[10]K. J. LaGattuta and Y. Hahn, Phys. Rev. A **25**, 411 (1982).
[11]Y. Hahn, Adv. At. Mol. Phys. **21**, 123 (1985).
[12]G. Omar and Y. Hahn (unpublished).
[13]G. Omar and Y. Hahn, Phys. Rev. A (to be published).